

Investigation of Doped Titanium Dioxide in Anatase Phase. Study *ab initio* using Density Functional Theory

Paulo José Pereira de Oliveira^{1,*}, Fabielle Castelan Marques, Arlan da Silva Gonçalves^{2,3}, Greice Kelly dos Santos Brito¹, Enzo Victorio Andrade¹, Marcos Pedro Dalmaso Pinto¹

¹Federal Institute of Education, Science and Technology of Espírito Santo – unit Cachoeiro de Itapemirim, ES, Brazil, 29300-970

²Federal Institute of Education, Science and Technology of Espírito Santo – unit Vila Velha, ES, Brazil, 29106-010

³Federal University of Espírito Santo – unit Vitória, ES, Brazil, 29075-910

*Corresponding author: E-mail: paulojoseo@ifes.edu.br; Tel: (+55) 28 999583818

DOI: 10.5185/amlett.2020.011459

Global warming has generated great concern worldwide. One way to control this problem is to use clean renewable energy new sources. Among the energy sources, we can mention hydrogen gas, produced by water photocatalysis by mean of a semiconductor material. In this work, we report a study about band gap and absorption spectra by mean of the density functional theory of the anatase allotropic form of titanium dioxide doped with Ruthenium. The results indicated systematic decrease of the band gap and increase of the absorbance at the visible region with the increase of the amount of dopant.

Introduction

Demand for energy supplies, high oil prices and rising greenhouse gas emissions are still unresolved challenges for the global economy and the planet's climate. Among the alternative energy sources, hydrogen production is an attractive option because releases high energy quantity per unit of mass and its combustion generate pure water [1].

Among the several technologies for the hydrogen production, we highlight the heterogeneous photocatalysis intermediated by semiconductors [2-4]. In the scientific world, titanium dioxide (TiO₂) is the most studied. It is found in nature under three allotropic forms: rutile, anatase and brookite. The anatase form is the most used in photocatalysis due to its better activity [5].

TiO₂ offers some advantages, such as: low cost, high stability, water insolubility and low toxicity [6-8]. However, TiO₂ is not able to decompose H₂O at the visible region, since it only absorbs radiation below of 387 nm (band gap of 3.2 eV) at the anatase phase [9]. Even in the ultraviolet region, the H₂ production is low when TiO₂ is used in pure water, due to high recombination rate of the generated photoelectrons, which ceases the photocatalytic effect after an illumination short period [10-12]. Many experimental and theoretical works have indicated that impurities introduction can improve the photocatalytic activity of TiO₂ [13-18]. Dopants of transition metals, such as Fe, V, Ni, Co and Cu, promotes the absorption deviation to the boundary of the red wavelength and decreases the rate of recombination of the generated photoelectrons [14, 19-21]. Non-metal dopants, such as C, N and S, diverts the top of the valence band to

higher energies, which reduces the band gap responding to visible light region [15, 22-24]. The interaction with precious metals of work function (ϕ) greater than that of TiO₂, such as Pt, Pd, Ru and Au, has been considered as the best alternative to suppress the recombination of charges facilitating charge transferring from the metal (or metallic oxide) to the semiconductor due to Schottky barrier formation at the junction between the surface of the materials and the occurrence of surface plasmon resonance [11]. Recently, Song and collaborators [25] investigated the doping of rutile TiO₂ with the following transition metals: Y, Nb, Mo, Tc, Ru, Rh, Pd, Ag and Cd, showing that the Ti atoms substitution by Nb or Mo results in an n-type semiconductor, reducing the rutile energy gap and causes shift to red of the optical absorption. Ti substitution by Tc, Ru, Rh and Pd, divides the energy gap into two subgaps and improves absorption in the visible. Zhao *et al.* [26] showed that the anatase TiO₂ doped with 3d transition metals (Sc, V, Cr, Mn, Fe, Co and Ni) approximates the Fermi level of the conduction band and consequently reduces the band gap and improves absorption in the visible.

Ruthenium dioxide (RuO₂) as well as other oxides of the transition metals family with structure similar to rutile, have been intensively investigated for photocatalysis due to their unique properties, such as chemical stability and good electrical conductivity [27-29]. Experimental works has indicated that RuO₂ in contact with TiO₂ increases the conductivity, improving charges separation at the metal-semiconductor interface allowing charge transferring inside of the photocatalyst of more efficiently form [30, 31].

Marques *et al.* observed an improvement in H₂ production by placing RuO₂ in contact with a TiO₂ anatase in MCM-41 molecular sieves [11]. Ismael [32] and Houšková *et al.* [33] also experimentally verified increase of photocatalytic activity and decrease in band gap when TiO₂ is doped with Ru.

Recently, Nemudzhvadi *et al.* investigated through DFT calculations the anatase TiO₂ (1 0 1) Surface doped with Ruthenium showing that doping reduces the band gap energy [34]. In this work we investigated the anatase TiO₂ doping with Ru using a new and different computational methodology. In order to analyze optical properties at the visible region, we calculate, besides the band gap, the absorption spectra for TiO₂ doped with different amounts of Ru dopants.

Computational methodology

Doping

Unit cell of Ti₄O₈ in the Anatase phase was retrieved from the Avogadro program database and [35] the following geometric parameters: $a = b = 3.785 \text{ \AA}$, $c = 9.514 \text{ \AA}$ e $\alpha = \beta = \gamma = 90^\circ$ were used. In order to perform the doping we investigated the distribution of the HOMO orbital of TiO₂ to verify the location of highest probability of Ti to be replaced by Ru. The first result was generated using the MOPAC2016 (PM7 method) [36, 38] and jmol [37] programs, showing that the HOMO orbital is concentrated on the Titanium atom on the left. Thus this atom was chosen for doping through of the isomorphic substitution of a Ti atom by a Ru atom, Fig. 1.

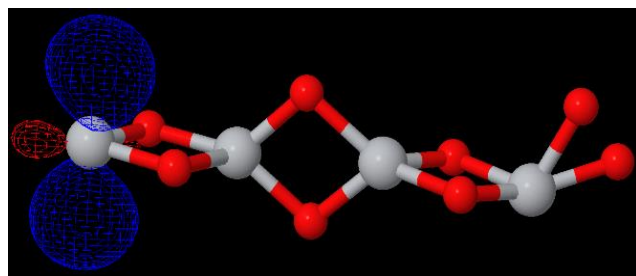


Fig. 1. Shows clearly that the homo orbital is concentrated on the Titanium atom in the left. Thus, this atom was chosen for doping through the isomorphic substitution of a Ti atom by a Ru atom. Figure 1 was generated using the MOPAC2016 (PM7 method) [36, 38] and jmol [37] programs.

Choice of functional

Energy band gap and visible absorption spectra were performed with the Siesta program [39]. The Siesta program is specific to crystal and uses the density functional theory (DFT) and the pseudopotential methodology. The pseudopotentials used in this work were acquired from the reference [40]. The choice of the exchange correlation functional of the DFT method used this work was done after analyzing the results obtained with three different functionals, Table 1.

Table 1. Fermi energy and direct band gap calculations in electron-volts (eV) for Ti₄O₁₂ for different Exchange-Correlation Functionals.

GGA	Fermi energy	Valencia Band (VB)	Conduction Band (CB)	band gap (CB-VB)
PBE ¹	-5.52	-6.94	-4.10	2.8
PBE ²	-5.18	-6.79	-3.68	-3.1
PBEJsJrLO ³	-5.73	-7.05	-4.21	-2.8

¹[41].

²Modified GGA-PBE functional, see reference [42].

³GGA-PBE functional with parameters β , μ and κ fixed by the jellium surface (Js), jellium response (Jr), and Lieb-Oxford bound (LO) criteria, respectively, see references [43] and [44].

After Table 1 analysis, we decided to choose the GGA/RPBE functional, since its proximity to the titanium dioxide experimental band gap data that is 3.2 eV [11]. These calculations were performed using a DZP base level, generated by Siesta with thermodynamic corrections for the temperature of 0.025 eV (290 K), an energy cut-off for the kinetic energy of the plane waves of 100 Ry (1360 eV) and the following symmetry points of 3.776Å to obtain the k points of the energy bands: R = (1, 1, 2.51), $\Gamma = (0.5, 0.5, 1.255)$, X = (0.5, 1, 1.255) and M = (1, 1, 1.255). Graph 1 shows the energy bands of the Ti₄O₁₂. We have developed an auxiliary program in Mathematica [45] to put the Siesta output data into a format to be plotted in the GRACE software [46].

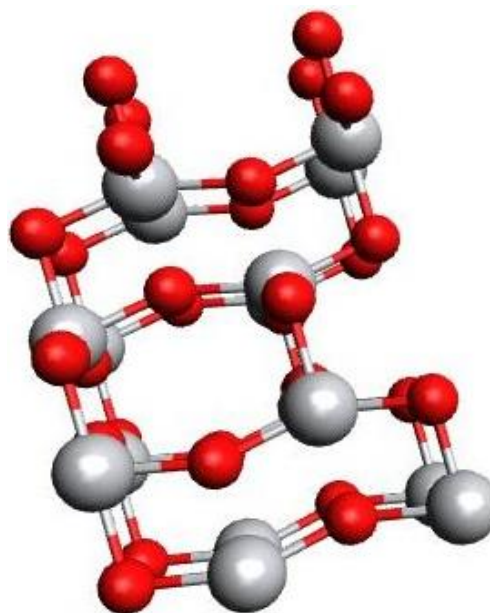


Fig. 2. Titanium dioxide supercell (2x2x1), with atoms 48 (Ti₁₆O₃₂).

Supercell

In order to analyze the doping effects we consider a titanium dioxide supercell (2x2x1), with atoms 48 (Ti₁₆O₃₂, see Fig. 2). It was obtained by folding the original Ti₄O₁₂ unit cell at the (a) and (b) directions. Thus,

the supercell parameters were: $a = b = 7.57 \text{ \AA}$, $c = 9.514 \text{ \AA}$ and $\alpha = \beta = \gamma = 90^\circ$. The symmetry points have become: $R = (2, 2, 2.51)$, $\Gamma = (1, 1, 1.255)$, $X = (1, 2, 1.255)$ and $M = (2, 2, 1.255)$. The functional used at the $\text{Ti}_{16}\text{O}_{32}$ supercell was the GGA/RPBE. This choice of functional was made based at the calculations obtained with the Ti_4O_{12} unit cell. The others calculation parameters, were kept identical to that of the original Ti_4O_{12} unit cell. **Fig. 3** show the doped supercell with four Ru. We allow a relaxation of the atomic coordinates of the no-doped and doped supercell performing geometry optimization with 150 steps, each measuring 0.037 \AA . We also allow SCF interactions two thousand for each DFT calculation to ensure energy convergence.

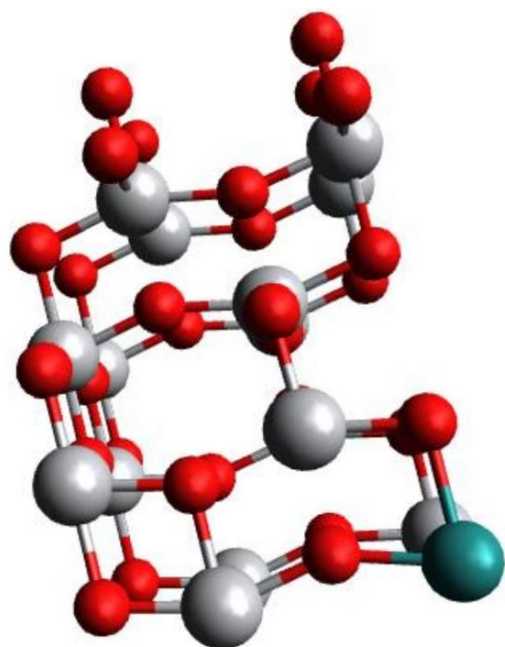


Fig. 3. Doped supercell with four Ru.

Results and discussion

Anatase presents a tetragonal crystalline system of centered body, where each cell unit contains four TiO_2 molecules intercalated. The titanium is coordinated by six oxygen atoms by two larger apical bonds and by four equatorial bonds of 1.979 \AA and 1.932 \AA at 15 K , respectively [47]. The anatase crystal is formed by distorted TiO_6 octahedral channels. In our study, the assigned bonding lengths were 1.92 \AA for equatorial bonds and 1.89 \AA for apical bonds. Although Ru and Ti have a preference by six coordinate number and both ions have formal charge of +4, this distortion can be caused by the difference in atom size. The effective ionic radius of Ru (IV) is higher (62.0 pm) than Ti (IV) (60.5 pm) in the hexacoordinate structure of anatase [48].

The results of the band gap calculations for doped and undoped $\text{Ti}_{16}\text{O}_{32}$ supercell are shown in **Fig. 4**. For the non-doped material, $E_g = 2.3 \text{ eV}$ which is underestimated by about 30% compared with the experimental value

of 3.2 eV , corroborating with the literature. The underestimation always exists in the band gap calculations due to the well-known limitation of the DFT theory [49]. However, the character of the band structure and the trend of the energy gap variations as a function of the Ruthenium concentration from the calculations are expected to be reasonable and reliable.

After the one Ti atom replacement Ru the band gap decreases to 1.1 eV . The replacement of two Ti atoms by two Ru atoms decreases the band gap energy to 0.3 eV . Finally, replacement of four Ti atoms by four Ru atoms decreases the band gap to 0.0 eV .

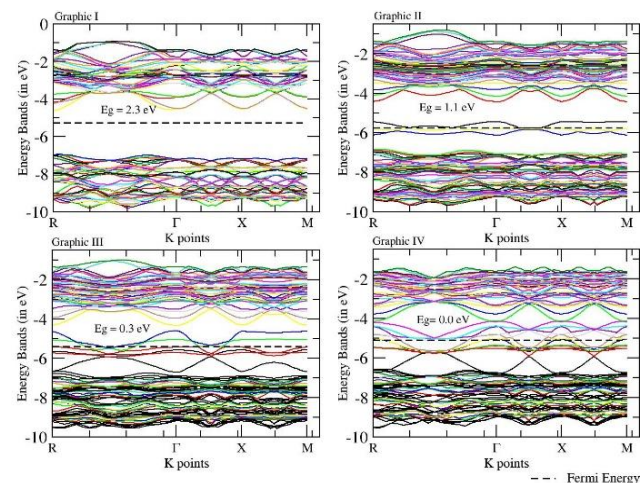


Fig. 4. Graph of the energy bands as a function of the K points for the $\text{Ti}_{16}\text{O}_{32}$ supercell before (Graphic I) and after the doping with one Ru atom (Graphic II), two Ru atoms (Graphic III) and four Ru atoms (Graphic IV).

An analysis of **Fig. 4** indicates a clear narrowing of the energy bands as the increases dopant number, showing that the material behaves as a conductor for higher quantities of Ru. **Fig. 4-I**, for the non-doped sample, shows that the Fermi level is approximately in the middle of the valence and conduction band agreeing with the literature [26]. **Fig. 4-II** and **Fig. 4-III**, doped with one and two Ru respectively, the Fermi level was shifted to just below of the top of the valence band, indicating that the substitution of Ru in anatase TiO_2 would transform the material into a p-type semiconductor. In **Fig. 4-IV**, occurs a superposition of the valence and conduction bands and it is no longer possible to distinguish the bands, so the material becomes conductor rather than semiconductor. Since Ru has an electron at the valence layer ($[\text{Kr}]4d^75s^1$), it behaves as an electron acceptor impurity and this could explain the shift from the Fermi level to just below of the valence band top. An analysis of **Fig. 4-I**, **Fig. 4-II**, **Fig. 4-III** and **Fig. 4-IV** also indicated that the band gap were direct (energy difference of the valence and conduction band concentrated at the same point k) at all symmetry points R, Γ , X and M, located at the following points in graph 0.00, 0.833, 1.273 and 1.71, respectively. Fermi, conduction band and valence band energies are showed in **Table 2**.

Table 2. Fermi and direct band gap energies calculations in electron-volts (eV) for $\text{Ti}_{16}\text{O}_{32}$ no doped and doped with one, two and four Ru respectively.

Supercell	Fermi energy	Valencia Band (VB)	Conduction Band (CB)	band gap (CB-VB)
$\text{Ti}_{16}\text{O}_{32}$	-5.27	-6.94	-4.63	2.31
$\text{Ti}_{15}\text{RuO}_{32}$	-5.74	-5.48	-4.43	1.05
$\text{Ti}_{14}\text{Ru}_2\text{O}_{32}$	-5.39	-4.61	-4.32	0.29
$\text{Ti}_{12}\text{Ru}_4\text{O}_{32}$	-5.14	-	-	0.0

Fig. 5 shows the results of optical absorption at the ultraviolet and visible spectrum. We consider an unpolarized electric field that is applied in the three spatial directions. The optical absorption is obtained from the imaginary part of the dielectric constant [50].

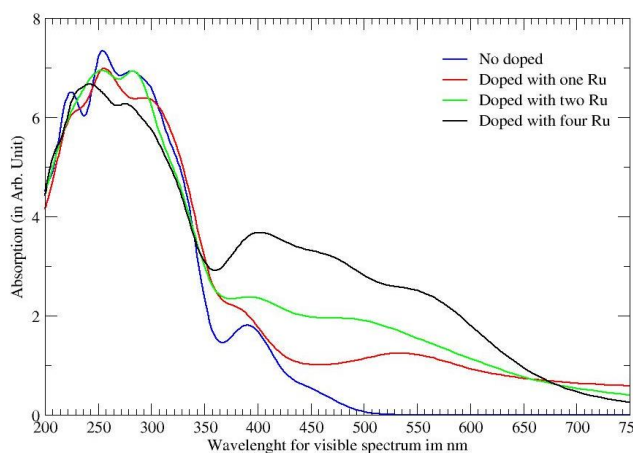


Fig. 5. Theoretical Optical absorption at the visible spectrum of the doped and non-doped Anatase supercell with Ru.

UV-Vis spectra shown, **Fig. 5**, that an intense absorption at the range between 200nm and 400nm is characteristic of the electronic transition $\text{O}(2p)\text{-Ti}(3d)$ (from the valence band to the conduction band) and is typical of TiO_2 anatase, with Ti^{4+} in octahedral coordination [51].

The ruthenium insertion in the crystalline structure increases its content, from 7.6% wt., in the case of the substitution of 1 atom of Ti in the supercell, for 14.6% wt. (2 Ru atoms) and 27,1% wt. (4 Ru atoms). After this doping, the absorption of energy at wavelengths greater than 400nm (visible region) increases with increasing Ru content. This can be attributed to the low photon energy and/or thermal excitation of electrons trapped in localized defects states, such as oxygen vacancy or ruthenium substitution sites that are located below of the conduction band. This absorption of wavelengths greater than 400nm are responsible for the decrease of the energy band gap. Authors reported that a strong absorption between 410 nm and 620 nm can be attributed to donors load transfer ($\text{Ru}^{4+} \rightarrow \text{Ru}^{5+} + e^-$, $\text{Ru}^{3+} \rightarrow \text{Ru}^{4+} + e^-$) or of acceptors ($\text{Ru}^{4+} \rightarrow \text{Ru}^{3+} + h^+$) [52,53]. Other authors also report that TiO_2 doping by Ru causes intermediate bands formation

and electronic transitions could arise mainly by $\text{O}(2p)\text{-Ru}(4d)$ orbitals and d-d in Ru 4d orbitals [48]. These transitions would result in lower band gap when compared to TiO_2 , a fact observed in this work. The formation of intermediate bands and/or bands with lower band gap values increases the photocatalytic activity of the material at the visible region, which makes it susceptible to sensitization using sunlight. Specifically the electronic transferring from VB to CB by photoexcitation makes it possible to perform water reduction reaction to produce H_2 fuel by water splitting.

Conclusion

In this work we investigated doping effect in anatase TiO_2 with Ru using the DFT method and the GGA/RBPE exchange correlation functional. Band gap and optical absorption calculations were performed for different amounts of Ru. Doping with Ru produces a narrowing of the band gap. The band gap systematically reduces as the amount of dopant increases (2.31 eV \rightarrow 1.05 eV \rightarrow 0.29 eV \rightarrow 0.0 eV), indicating that the material ideally becomes heterogeneous (semiconductor) photocatalyst for low Ru concentrations. The doping with Ru causes the material to behave like a p-type semiconductor, because it causes the displacement of the Fermi level to near the valence band.

The visible spectrum absorption range also increases considerably with the presence of Ru, expanding the absorption spectrum of anatase to the solar spectrum region. Finally, the results indicate that Ru is a potential impurity capable of sensitizing anatase with visible light and acting as a photocatalyst for applications involving photocatalysis for the production of hydrogen via water-splitting in a clean and renewable way.

Acknowledgements

We would like to acknowledge the financial support of the FAPES (Brazilian Agency). We would like to thank too our friend Osmair Vital de Oliveira* for his valuable suggestions for completing this work.

*Federal Institute of Education, Science and Technology of São Paulo, Campus Catanduva.

Author's contributions

Performed the calculations: Greice, Enzo and Marcos Pedro
Wrote the paper: Fabielle, Paulo, Arlan
Authors have no competing financial interests: No

Keywords

Band gap, DFT, photocatalysis, titanium dioxide.

Received: 29 July 2019

Revised: 11 October 2019

Accepted: 23 October 2019

References

- Smith, R. J. B.; Shantha, M. S.; *Int. J. Chem. React. Eng.*, **2007**, *5*, 1.
- Ni, M.; Leung, M. K. H.; Leung, D. Y. C.; *Renewable Sustainable Energy Rev.*, **2007**, *11*, 401.
- Patsoura, A.; Kondarides, D. I.; Verykios, X. E.; *Catal. Today*, **2007**, *124*, 94.

4. Strataki, N.; Bekiari, V.; Kondarides, D. I.; Lianos, P.; *Appl. Catal.*, **2007**, B, 77, 184.
5. Ziolli, R. L.; Jardim, W. F.; *Quim. Nova*, **1998**, 21, 319.
6. Ni, M.; Leung, M. K. H.; Leung, D. Y. C.; Sumathy, K. A.; *Renew Sustain Energy Rev.*, **2007**, 11, 401.
7. Galinska, A.; Walendziewski, J.; *Energ. Fuel*, **2005**, 19, 1143.
8. NL, W.; MS, L.; *Int J. Hydrog Energy*, **2004**, 29, 1601.
9. Linsebigler, A. L.; Guangquan, L.; Yates J. T.; *Chem Rev.*, **1995**, 95, 735.
10. Leung, D. Y.; Fu, X.; Wang, C.; Ni, M.; Leung, M. K.; Wang, X.; Fu, X.; *ChemSusChem*, **2010**, 3, 681.
11. Marques, F. C.; Canela M. C.; Stumbo A. M.; *Topics in Catalysis*, **2017**, 60, 1196.
12. Maeda, K.; *J. Photochem. Photobiol. C.*, **2011**, 12, 237.
13. Li C.; Zhao, Y. F.; Gong, Y. Y.; Wang, T.; Sun, C. Q.; *Phys. Chem. Chem. Phys.*, **2014**, 11, 21446.
14. Pan, J.W.; Li, C.; Zhao, Y.F.; Liu, R.X.; Gong, Y.Y.; Niu, L.Y.; Liu, X.J.; Chi, B.Q.; *Chem. Phys. Lett.*, **2015**, 628, 43.
15. Han, X.P.; Shao, G.S.; *J. Phys. Chem. C*, **2011**, 115, 8274.
16. Romero-Gomez, P.; Lopez-Santos, C.; Borrás, A.; Espinos J.P.; Palmero, A.; Gonzalez-Elipse, A.R.; *Chem. Phys. Lett.*, **2014**, 582, 95.
17. Samet, L.; Nasseur, J.B.; Chtourou, R.; March, K.; Stephan, O.; *Mater. Charact.*, **2013**, 85, 1.
18. Spadavecchia, F.; Cappelletti, G.; Ardizzone, S.; Ceotto, M.; Falciola, L.; *J. Phys. Chem. C*, **2011**, 115, 6381.
19. Long, R.; English, N.J.; *Chem. Phys. Lett.*, **2009**, 478, 175.
20. Wang, S.; Yang, X.J.; Jiang, Q.; Lian, J.S.; *Mater. Sci. Semicond. Process.*, **2014**, 24, 247.
21. Inturi, S.N.R.; Boningari, T.; Suidan, M.; Smirniotis, P.G.; *Appl. Catal. B: Environ.*, **2014**, 144, 333.
22. Harb, M.; Sautel, P.; Raybaud, P.; *J. Phys. Chem. C.*, **2013**, 144, 8892.
23. Xin, G.; Pan, H.P.; Chen, D.; Zhang, Z.H.; Wen, B.; *J. Phys. Chem. Solids.*, **2013**, 74, 286.
24. Wang, S.; Zhao, L.; Bai, L.; Yan, J.; Jiang, Q.; Lian, J.S.; *J. Mater. Chem.*, **2014**, A 2, 7439.
25. Song, K.; Han, X.; Shao, G.; *Journal of Alloys and Compounds*, **2013**, 551, 118.
26. Zhao, Y. F.; Li, C.; Lu, S.; Yan, L. J.; Gong, Y. Y.; Niu, L. Y.; Liu, X. J.; *Chem. Phys. Letters*, **2016**, 647, 36.
27. Yuan, Y. P.; Ruan, L. W.; Barber, J.; Loo, S. C. J.; Xue C.; *Energy Environ. Sci.*, **2014**, 7, 3934.
28. Dahl, M.; Liu, Y.; YIN, Y.; *Chem. Rev.*, **2014**, 114, 9853.
29. Kubacka, A.; Fernández-García, M.; Colón, G.; *Chem. Rev.* **2012**, 112, 1555.
30. Sakata, T.; Hashimoto, K.; Kawai, T.; *J. Phys. Chem.*, **1984**, 88, 5214.
31. Blondeel, J.; Harriman, A.; Poter, G.; Urwin, D.; Kiwi, J.; *Phys. Chem.*, **1983**, 87, 2629.
32. Ismael, M.; *New J. Chem.*, **2019**, 43, 9596.
33. Houšková, V. et al., *Cent. Eur. J. Chem.*, **2009**, 7, 259.
34. Nemudzhvadi, H.; et al.; *J. Phys.: Conf. Ser.*, **2017**, 905, 012013.
35. Ali, S.; et al., Avogadro: Molecular Editor and Visualization, Release 1.1.1, 2013. See <https://avogadro.cc/>.
36. MOPAC2016, J.J.P. Stewart, Stewart Computational Chemistry, Colorado Springs, CO, USA.
37. Jmol: an open-source Java viewer for chemical structures in 3D. <http://www.jmol.org/>.
38. Mopac, on-line manual, keyword GRAPHF. <http://openmopac.net/manual/graph.html>, (accessed 29 October **2018**).
39. Artacho, E.; Cela, J. M.; Gale, J.; Garcia, A.; Junquera, J.; Martin, R. M.; Ordejón, P.; Sánchez-Portal, D.; Soler, J. M.; *J. Phys. Cond. Matt.*; **2002**, 14, 2745.
40. GGA Pseudopotential Database. <https://departments.icmab.es/leem/siesta/Databases/Pseudopotentials/periodictable-gga-abinit.html>, (accessed 21 August **2018**).
41. Perdew, J. P.; Burke, K.; Ernzerhof, M.; *Phys. Rev. Lett.*, **1996**, 77, 3865.
42. Hammer, B.; Hansen, L. B.; Norskov, J. K.; *Phys. Rev. B.*, **1999**, 59, 7413.
43. Pedroza, L. S.; da Silva, A. J. R.; Capelle, K.; *Phys. Rev. B.*, **2009**, 79, 201106.
44. Odashima, M. M.; Capelle, K.; Trickey, S. B.; *J. Chem. Theory Comput.*, **2009**, 5, 798.
45. Wolfram Research, Inc., Mathematica, Version 9.0, Champaign, IL (**2012**).
46. Turner, P. J.; XMGRACE, Version 5.1.25. Center for Coastal and Land-Margin Research, Oregon Graduate Institute of Science and Technology, Beaverton, OR; **2005**.
47. Wu, L.; Yu, J.C.; Fu, X.Z.; *J. Mol. Catal. A Chemical*, **2006**, 244, 25.
48. Nguyen-phan, T. D.; et al., *ACS Catalysis*. **2016**, 6, 407.
49. Shao, G. J.; *Phys. Chem. C.*; **2008**, 112, 18677.
50. Tian, F.; Liu, C.; *J. Phys. Chem. B* **2006**, 110, 17866.
51. Cambor, M. A.; Corma, A.; Matinez, A.; Pérez-Pariente, J.; *Chemical Communications*. **1992**, 8, 589.
52. Triggs, P.; Lévy, F.; *Phys. Stat. Sol. B.*; **1985**, 129, 363.
53. Salvador, P.; Gutiérrez, C.; Triggs, P.; Lévy, F; *Mater. Res. Bull.* **1984**, 19, 634.